Electronic Supplementary Information

Ru-O Covalency Regulated via Constructing RuO_2/Cr_2O_3 Heterogeneous Interface to Boosted Acidic Water Oxidation

Longquan Li[a], Xuanzhi Liu[a], Meihuan Liu[a], Pengfei Tan*[a], Binhua Zhou[a], Yue Yu[a], Feng Liu*[b], Jun Pan*[ab]

[a] State Key Laboratory of Powder Metallurgy, Central South University, 410083, Changsha, P. R. China

[b] Yunnan Precious Metals Lab Co., Ltd., Kunming, Yunnan 650106, China

1.Experimental section

1.1 Materials

Ruthenium chloride hydrate ($RuCl_3 \cdot xH_2O$), Chromium(III) nitrate nonahydrate ($Cr(NO_3)_3$ $9H_2O$, 99%), 2-Aminoterephthalic acid ($C_8H_7NO_4$, 98%), ruthenium oxide (RuO_2, AR, 99.9%) were purchased from Aladdin. N, N dimethylformamide (C_3H_7NO, A.R.) and sodium hydroxide (NaOH, AR, 98%) were purchased from Macklin. Nafion perfluorinated resin solution (5 wt. %) were purchased from Suzhou Sinero Technology Co., Ltd. Ethanol (CH_3CH_2OH, A.R.) were purchased from Tianjin Fuyu Fine Chemical Co., Ltd. The H_2SO_4 (GR, 98 wt. %) and were purchased from Sinopharm Chemical Reagent Co., Ltd. Conductive carbon paper (TGP-H-060 hydrophilicity) were Purchased from Toray. The water used in all experimental was ultrapure (Merck, 18.25 MΩ/cm).

1.2 Synthesis

In a typical RuO_2/Cr_2O_3 synthesis, 0.2 mmol $Cr(NO_3)_3 \cdot 9H_2O$, 0.3 mmol $RuCl_3 \cdot xH_2O$, and 0.2 mmol NH_2-BDC (2-Aminoterephthalic acid) were dissolved in 15 mL of deionized water and sonicated to form a homogeneous solution. Subsequently, 0.5 mmol NaOH was added to the solution and stirred. The resulting mixture was transferred into a Teflon-lined hydrothermal autoclave and heated at 150 °C for 12 hours. After cooling to room temperature, the product was washed twice with N, N-dimethylformamide (DMF) and ethanol, then air-dried at 80 °C overnight. Finally, the dried product was calcined in a muffle furnace at 400 °C with a heating rate of 5 °C/min and maintained at this temperature for 4 hours. After cooling to room

temperature, the final product was collected. The synthesis method for RuO_2, Cr_2O_3 was without $Cr(NO_3)_3 \cdot 9H_2O$ and $RuCl_3 \cdot xH_2O$.

1.3 Characterizations of catalysts

The crystal structures were characterized by X-ray diffraction (XRD, Smartlab SE, Cu Ka1). The microstructures and composition are studied using a scanning electron microscope (TESCAN), Transmission electron microscopy (FEI TF20), and an energy dispersive spectrometer (Super-X). Chemical shifts were characterized by X-ray photoelectron spectroscopy (Thermo Scientific K-Alpha). The XPS data were further analyzed using Avantage software. Operando Raman tests were carried out using a DXR3 Raman system (532 nm) and a CHI 760E electrochemical workstation. The spectra were processed and analyzed by the software codes Athena and Artemis. Electron paramagnetic resonance (Bruker EMXplus-6/1) was used to verify the presence of oxygen vacancies.

1.4 Electrochemical measurements

All electrochemical measurements were performed in a three-electrode cell connected with an electrochemical station (CHI 760E) at room temperature. The prepared samples were made into ink drops on carbon paper as working electrodes. A Pt foil and saturated calomel electrode (SCE) were used as the counter electrode and reference electrode, respectively. All potentials in this work were mentioned versus reversible hydrogen electrode (RHE) according to the Nernst equation:

$$E_{RHE} = E_{SCE} + 0.059 * pH + 0.241$$

Before performing electrochemical tests，the carbon paper was soaked in a

mixed solution of concentrated sulfuric acid and concentrated nitric acid (3:1, v/v) for 24 h for hydrophilic treatment. During electrochemical measurements on carbon paper, the catalyst ink was sprayed onto it using the drip coating method。In a typical procedure, the catalyst (2.0 mg) was dispersed in a mixture of 150.0 μL ethanol and 90.0 μL of deionized water, and then 10.0 μL of 5 wt. % Nafion aqueous solution was added. After 30 min of sonication, 50.0 μL of homogeneous ink was drop on 1.0 cm × 1.0 cm carbon paper and dried in room temperature air.

Before the formal test, the working electrode was first scanned from 0.9 to 1.5 V (vs. SCE) at a rate of 20 mV s^{-1} for 10 cycles to achieve stable cyclic voltammetry (CV) scans in 0.5 M H_2SO_4. Linear Sweep Voltammetry (LSV) curves were obtained at a scan rate of 5 mV s^{-1} with 95 % iR compensation. Electrochemical impedance spectroscopy (EIS) was performed at 1.23 V (vs. SCE) in a frequency range of 0.1 Hz to 10^5 Hz. And in-situ EIS plots were collected from 1.15 V to 1.4 V in a amplitude of 50 mV. The stability of RuO_2/Cr_2O_3 was measured by CP at current density of 10 mA cm^{-2}. The double layer capacitances (C_{dl}) were estimated by measuring the CV under different scan rates (20 mV s^{-1} -100 mV s^{-1}) in the range of 0.6 ~ 0.7 V (vs. SCE) potential. Electrochemical surface area (ECSA) was calculated by the following equation:

$$ECSA = C_{dl} / C_s$$

where C_s is the specific capacitance of the sample and the general value of C_s = 0.035 mF cm^{-2} was adopted according to previous studies.

2. Supplementary Figures

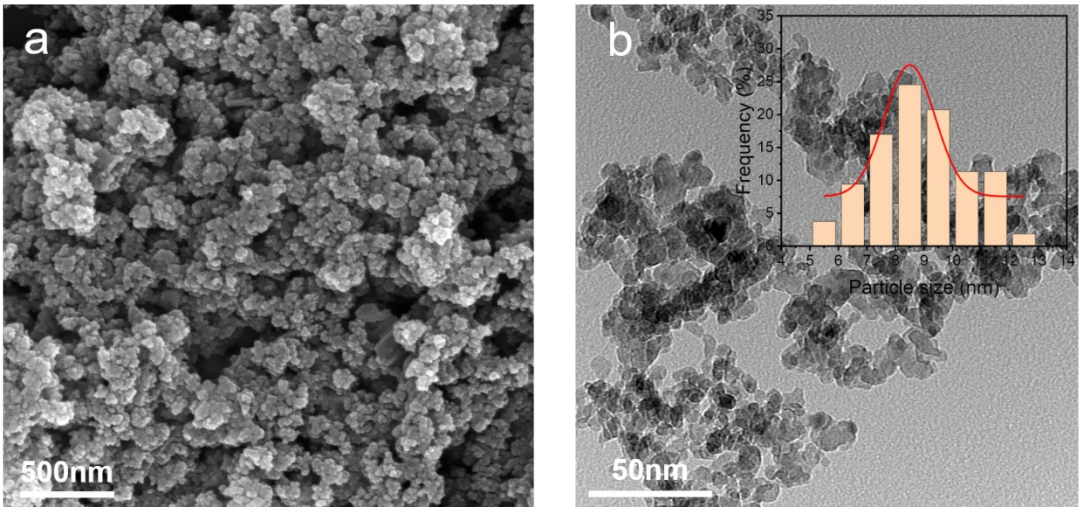

Figure S1. SEM images (a) and TEM images and particle size distributions of RuO_2/Cr_2O_3

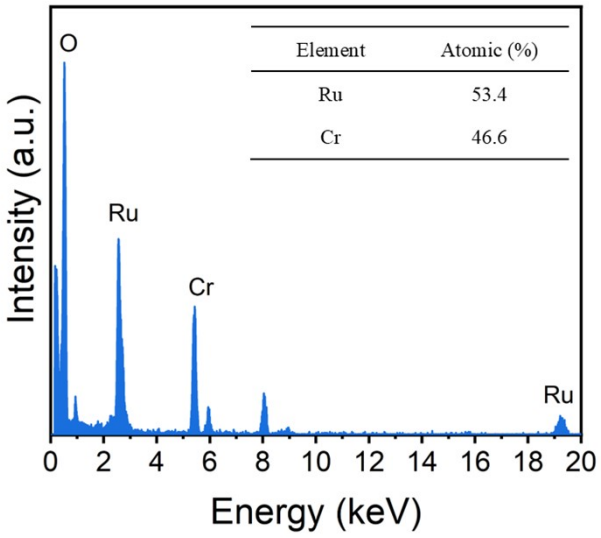

Figure S2. EDS results of RuO_2/Cr_2O_3

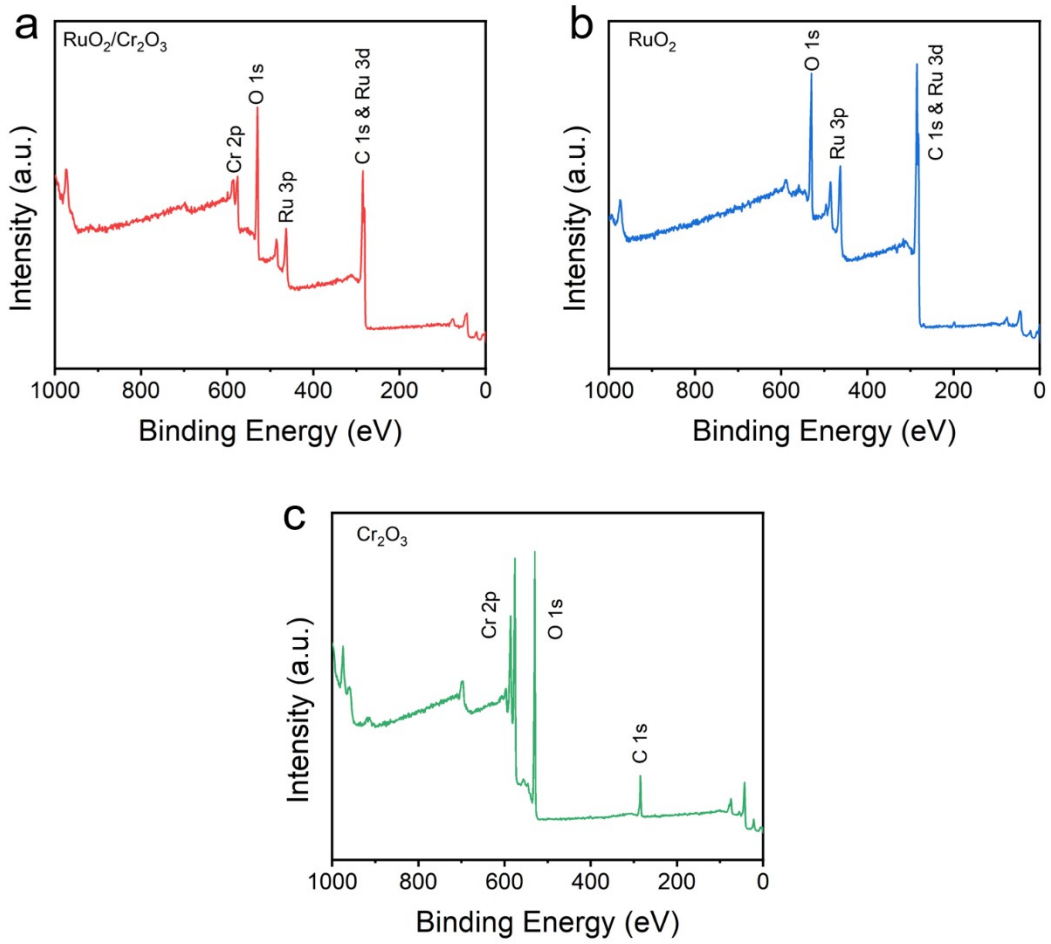

Figure S3. XPS survey spectra of RuO_2/Cr_2O_3, RuO_2 and Cr_2O_3

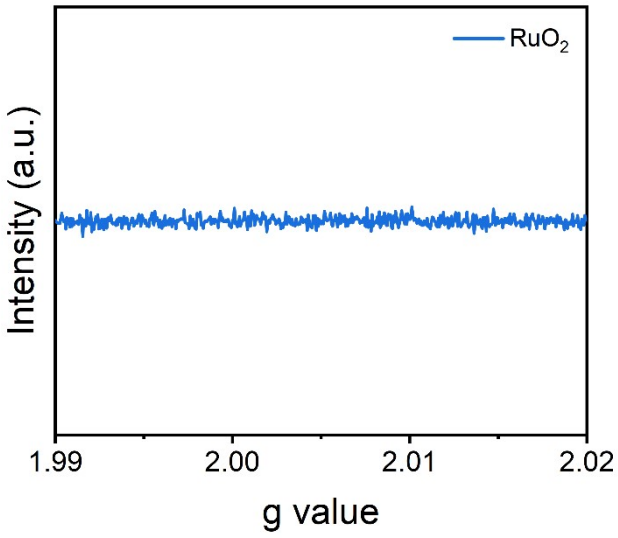

Figure S4. EPR spectra of RuO_2

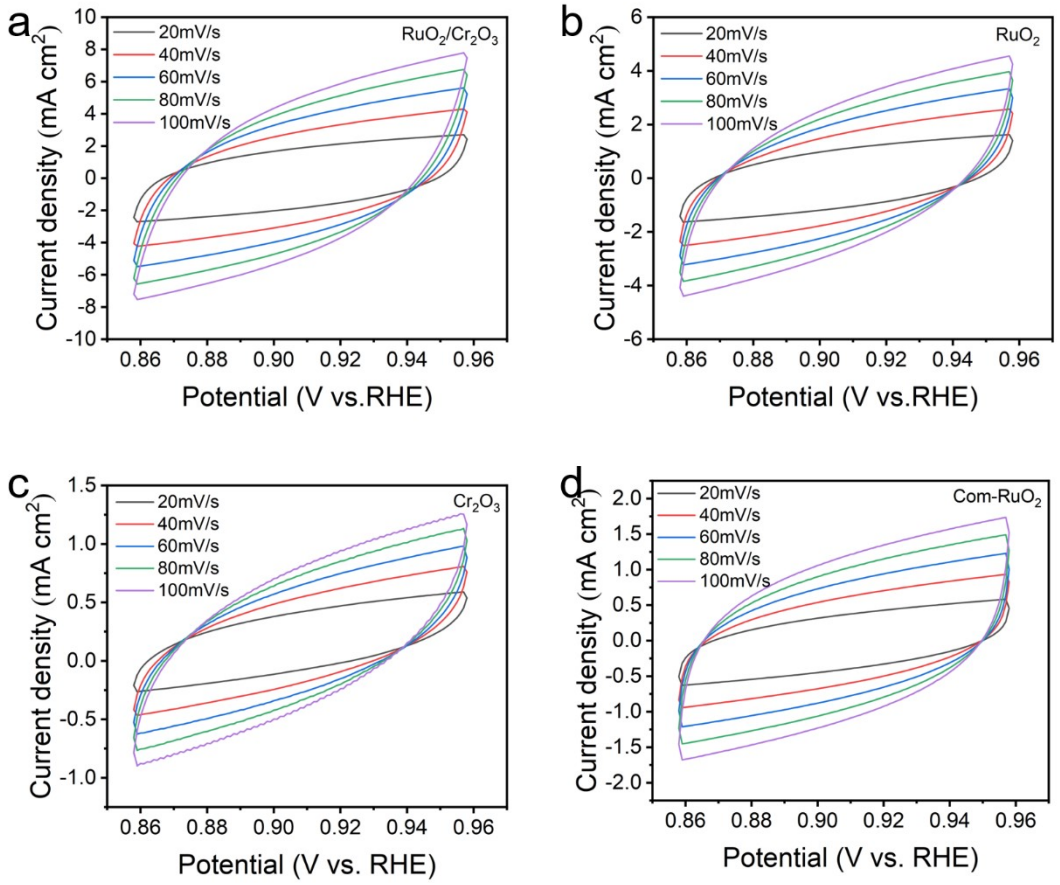

Figure S5. CV curves for these prepared samples: (a) RuO_2/Cr_2O_3; (b) RuO_2; (c) Cr_2O_3 (d) Com-RuO_2.

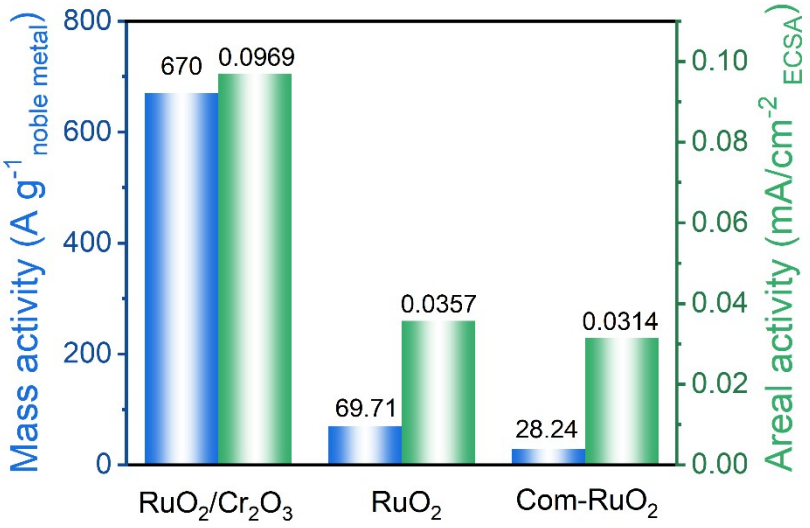

Figure S6. Mass activity and areal activity of RuO_2/Cr_2O_3 compared to RuO_2 and Com- RuO_2.

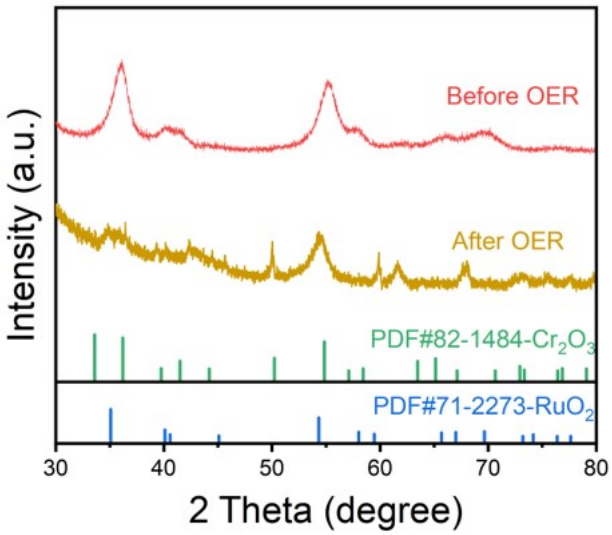

Figure S7. XRD pattern of the of RuO_2/Cr_2O_3 before and after OER testing.

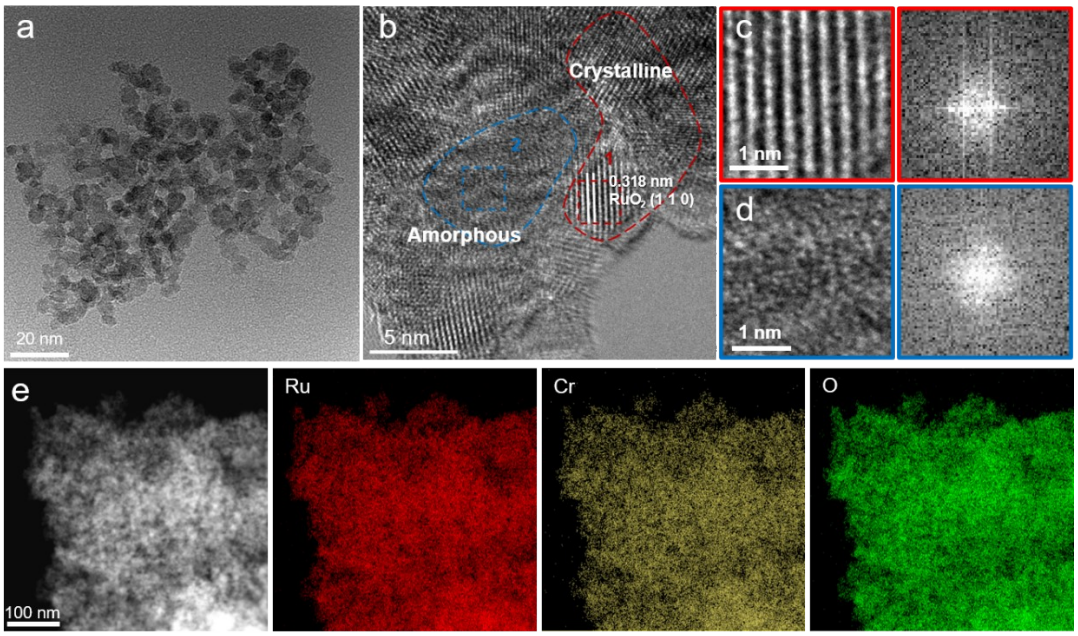

Figure S8. (a) TEM image of RuO_2/Cr_2O_3 after OER tests. (b) HRTEM image of RuO_2/Cr_2O_3 after OER tests. Enlarged images of the selected region 1 (c) and region 2 (d) and the corresponding FFT patterns. (e) HAADF-STEM image and corresponding EDS elemental mapping of RuO_2/Cr_2O_3 after OER tests.

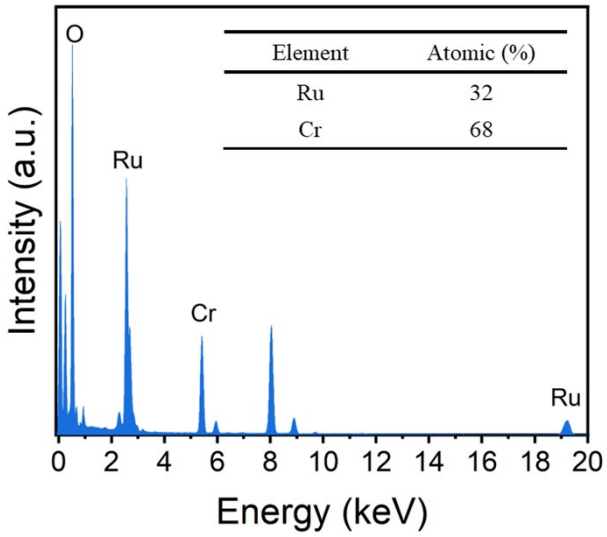

Element	Atomic (%)
Ru	32
Cr	68

Figure S9. EDS results of RuO_2/Cr_2O_3 after OER tests.

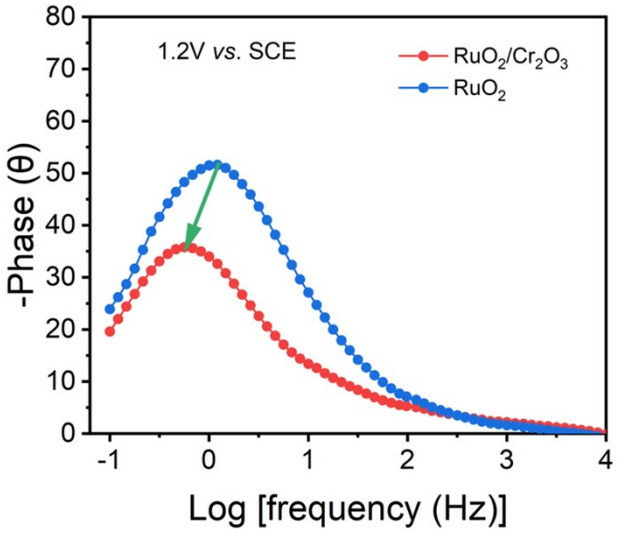

Figure S10. Bode phase plots of RuO_2/Cr_2O_3 and RuO_2 at 1.2 V versus SCE.

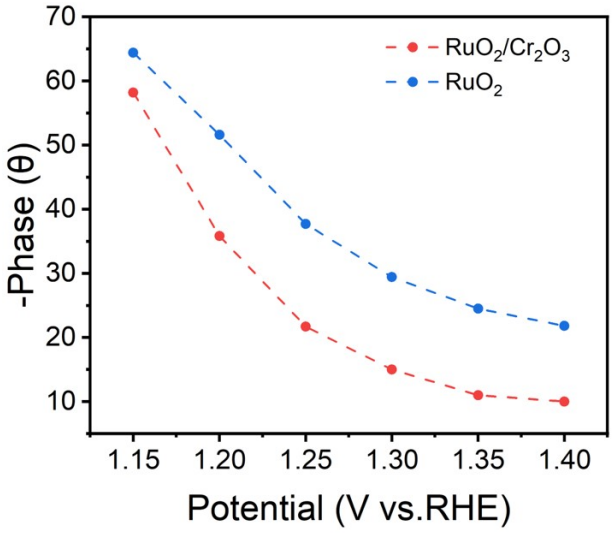

Figure S11. Response of the phase angle to the applied potential of RuO_2/Cr_2O_3 and RuO_2.

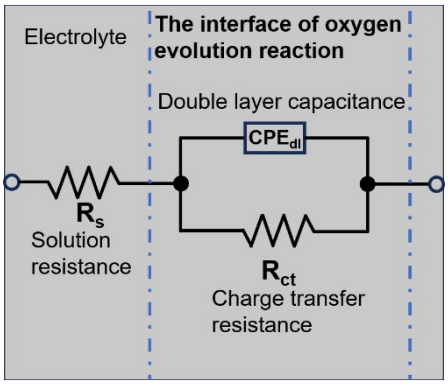

Figure S12. The electrochemical circuit. R_s is the solution resistance, R_{ct} is the polarization resistance, C_{dl} is the double-layer capacitance.

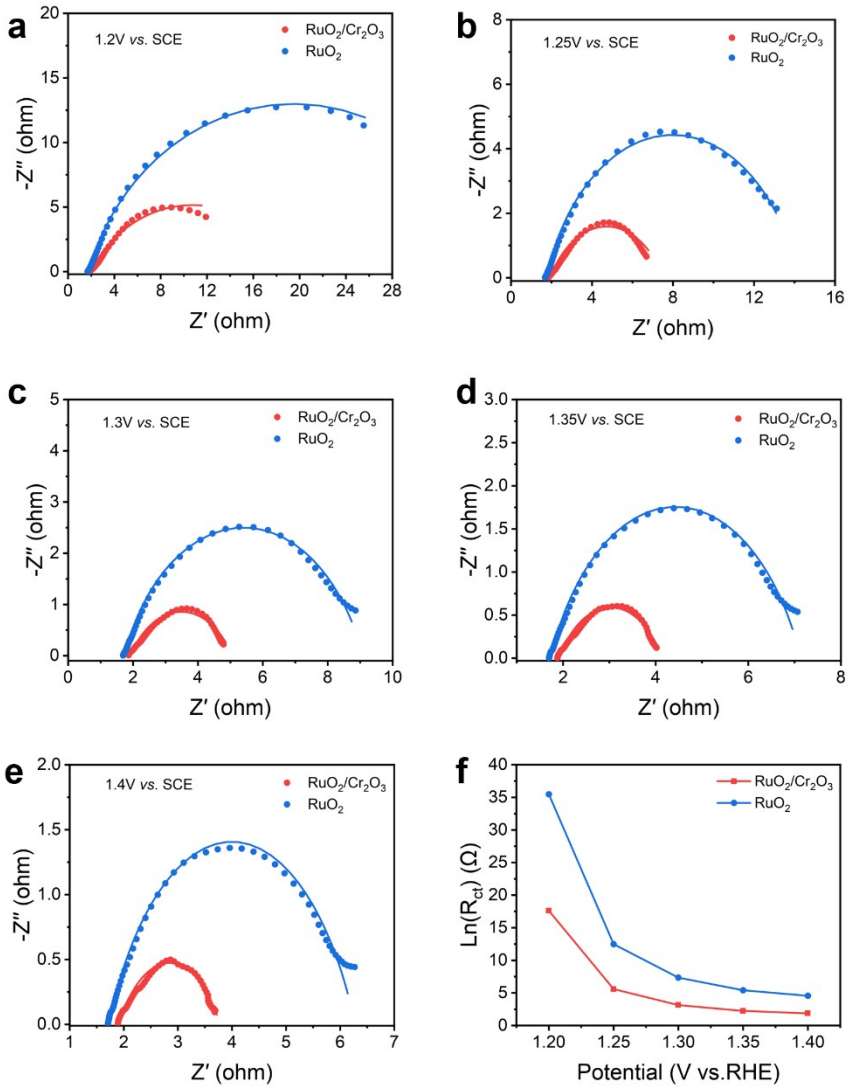

Figure S13. RuO_2/Cr_2O_3 and RuO_2 at different applied potentials versus SCE in 0.5 M H_2SO_4, (a) 1.2 V, (b) 1.25 V, (c) 1.3 V, (d) 1.35 V, (e) 1.4 V and (f) R_{ct} values at different potential for RuO_2/Cr_2O_3 and RuO_2.

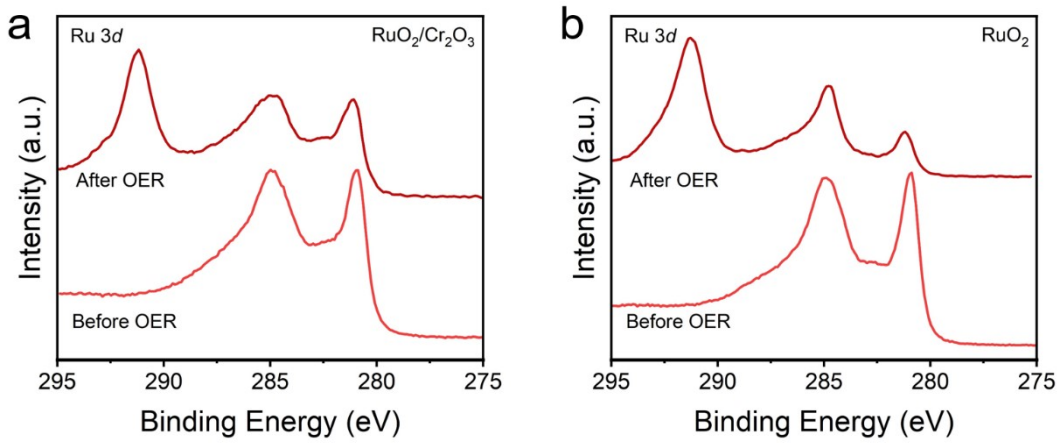

Figure S14. High-resolution Ru 3d XPS of (a) RuO_2/Cr_2O_3 and (b) RuO_2 before and after OER testing.

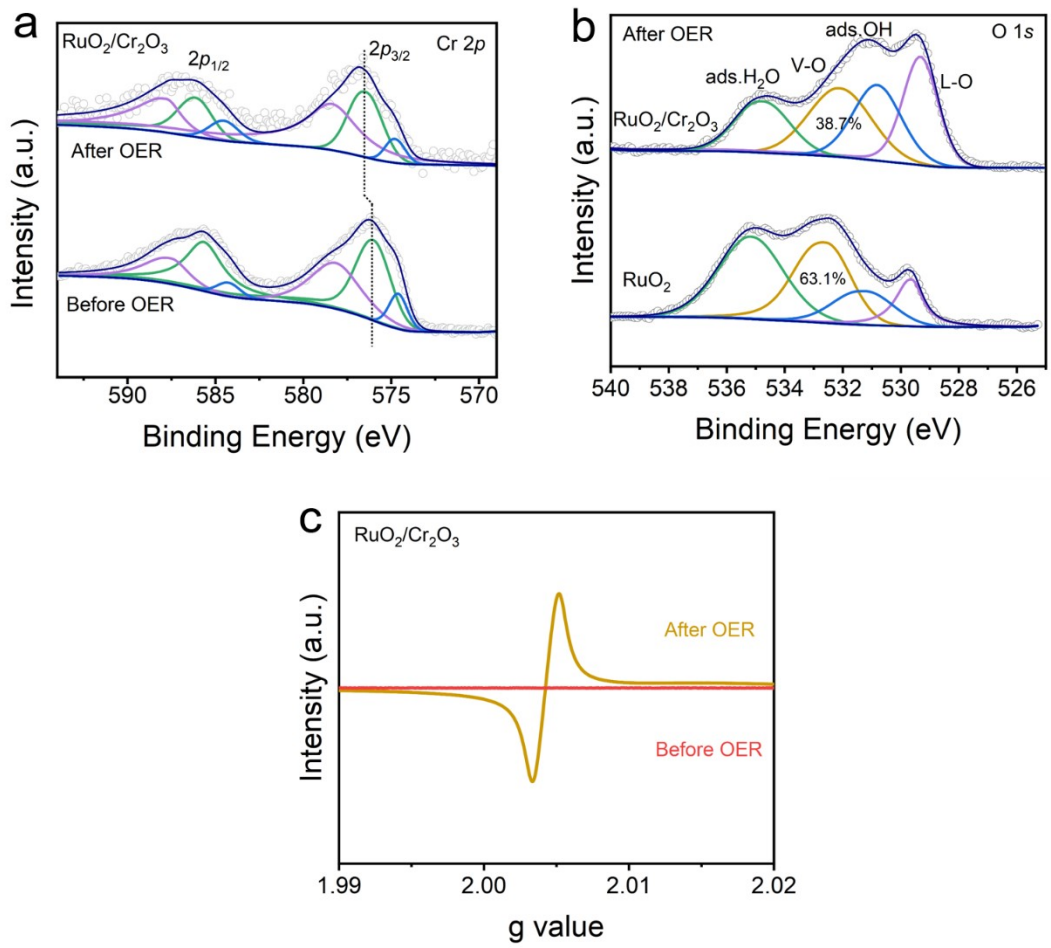

Figure S15. (a) High-resolution Cr 2p XPS of RuO_2/Cr_2O_3 before and after OER testing. (c) O 1s spectra for RuO_2/Cr_2O_3 and RuO_2 after OER testing. (c) EPR spectra of RuO_2/Cr_2O_3 before and after OER testing.

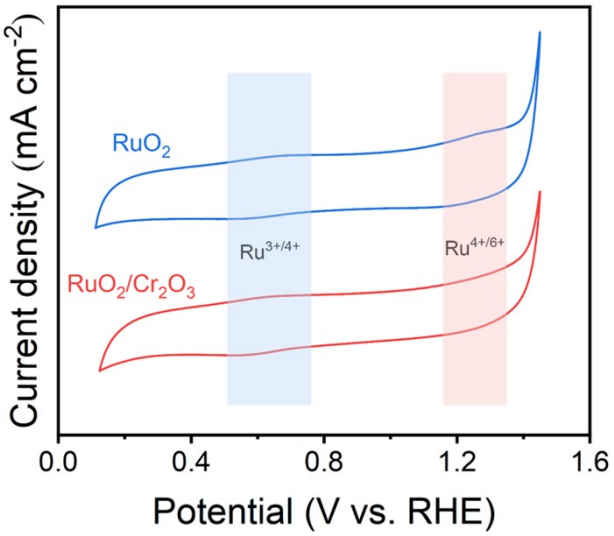

Figure S16 CV curves of RuO_2 and RuO_2/Cr_2O_3 catalysts in 0.5 M H_2SO_4 solution.

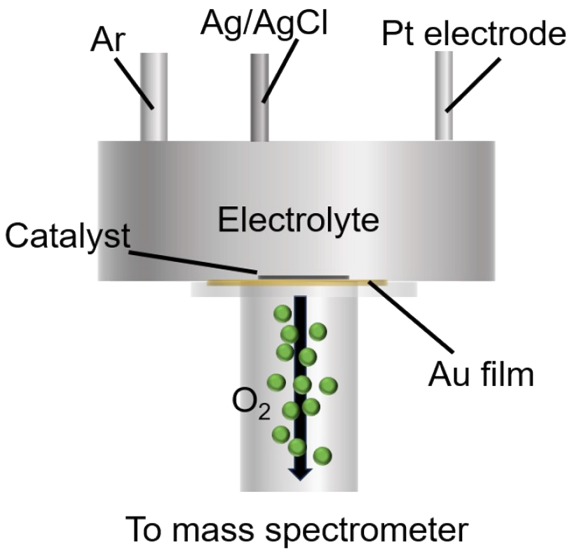

Figure S17. Schematic illustration of the operando DEMS.

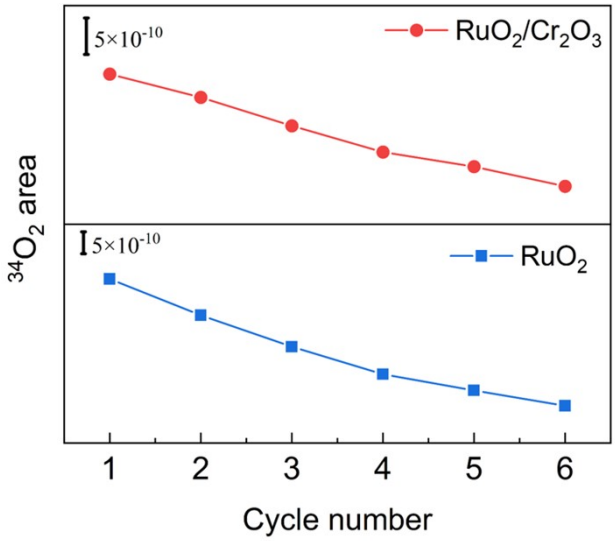

Figure S18. Area of $^{34}O_2$ DEMS signals for RuO_2/Cr_2O_3 and RuO_2 during six cycles in the potential range of 1.2–1.6 V versus RHE at a scan rate of 10 mV s^{-1}

3. Supplementary Tables

Table S1. ICP results of the concentration of each ion of RuO_2/Cr_2O_3.

Items	Content(at%)	
	Ru	Cr
RuO_2/Cr_2O_3	51	49

Table S2. The comparison of ECSA.

Catalysts	C_{dl} (mF cm^{-2})	ECSA (cm^2)
RuO_2/Cr_2O_3	37.78	1079.42
RuO_2	20.75	592.85
Com-RuO_2	9.56	273.14

ECSA is deduced from C_{dl} by dividing a factor of 0.035 mF cm^{-2}

Table S3. Parameters obtained by fitting EIS experimental spectra recorded at 1.23 V (vs. SCE).

Catalysts	Rs (ohm)	Rct (ohm)	CPE-T	CPE-P
RuO_2/Cr_2O_3	1.558	3.447	7.8E-02	6.8E-01
RuO_2	1.453	6.297	3.8E-02	7.6E-01
Com-RuO_2	1.851	11.43	2.4E-02	7.7E-01

Table S4 Comparison of OER activity with some representative electrocatalysts in acidic media.

Catalysts	Electrolyte solution	Overpotential at 10 mA cm^{-2} (mV)	Stability	References
RuO_2/Cr_2O_3	0.5 M H_2SO_4	218	30 h @ 10 mA cm^{-2}	This work
PdCu/Ir	0.1 M $HClO_4$	283	15 h @ 10 mA cm^{-2}	1
Co-RuIr	0.1 M $HClO_4$	235	25 h @ 10 mA cm^{-2}	2
Ru@IrOx	0.5 M H_2SO_4	282	2 h @ 10 mA cm^{-2}	3
RuB_2	0.5 M H_2SO_4	223	10 h @ 10 mA cm^{-2}	4
$Pt/Ni/RuO_2$	0.1 M $HClO_4$	239	N/A	5
IrO_2/MoO_3	0.1 M $HClO_4$	345	11 h @ 10 mA cm^{-2}	6
La-RuO_2	0.5 M H_2SO_4	208	28 h @ 10 mA cm^{-2}	7
Ru-N-C	0.5 M H_2SO_4	267	30 h @ 1.5V vs. RHE	8
6H-$SrIrO_3$	0.5 M H_2SO_4	248	30 h @ 10 mA cm^{-2}	9
$Y_{1.7}Sr_{0.3}Ru_2O_7$	0.5 M H_2SO_4	264	28 h @ 10 mA cm^{-2}	10
IrOx-B	0.1 M $HClO_4$	292	10 h @ 10 mA cm^{-2}	11
RuNi NAs	0.5 M H_2SO_4	252	10 h @ 10 mA cm^{-2}	12
Ir-doped WO_3	0.5 M H_2SO_4	258	60 h @ 100 mA cm^{-2}	13

$BaYIrO_6$	0.1 M $HClO_4$	315	1 h @ 10 mA cm^{-2}	14
$Ir_{0.06}Co_{2.94}O_4$	0.1 M $HClO_4$	300	200 h @ 10 mA cm^{-2}	15
IrTe NTs	0.5 M H_2SO_4	271	24 h @ 10 mA cm^{-2}	16
Ir-$NiCo_2O_4$	0.5 M H_2SO_4	240	70 h @ 10 mA cm^{-2}	17
$IrO_x/SrIrO_3$	0.5 M H_2SO_4	270	30 h @ 10 mA cm^{-2}	18
La_3IrO_7-SLD	0.1 M $HClO_4$	296	17 h @ 10 mA cm^{-2}	19

Supplementary References

1. M. Li, Z. Zhao, Z. Xia, M. Luo, Q. Zhang, Y. Qin, L. Tao, K. Yin, Y. Chao, L. Gu, W. Yang, Y. Yu, G. Lu and S. Guo, Exclusive Strain Effect Boosts Overall Water Splitting in PdCu/Ir Core/Shell Nanocrystals, *Angew. Chem. Int. Edit.*, 2021, **60**, 8243-8250.
2. J. Shan, T. Ling, K. Davey, Y. Zheng and S.-Z. Qiao, Transition-Metal-Doped RuIr Bifunctional Nanocrystals for Overall Water Splitting in Acidic Environments, *Adv. Mater.*, 2019, **31**, 1900510.
3. J. Shan, C. Guo, Y. Zhu, S. Chen, L. Song, M. Jaroniec, Y. Zheng and S.-Z. Qiao, Charge-Redistribution-Enhanced Nanocrystalline Ru@IrO_x Electrocatalysts for Oxygen Evolution in Acidic Media, *Chem.*, 2019, **5**, 445-459.
4. D. Chen, T. Liu, P. Wang, J. Zhao, C. Zhang, R. Cheng, W. Li, P. Ji, Z. Pu and S. Mu, Ionothermal Route to Phase-Pure RuB_2 Catalysts for Efficient Oxygen Evolution and Water Splitting in Acidic Media, *ACS Energy Lett.*, 2020, **5**, 2909-2915.
5. A. Oh, H. Y. Kim, H. Baik, B. Kim, N. K. Chaudhari, S. H. Joo and K. Lee, Topotactic Transformations in an Icosahedral Nanocrystal to Form Efficient Water-Splitting Catalysts, *Adv. Mater.*, 2019, **31**, 1805546.
6. M. Tariq, W. Q. Zaman, W. Sun, Z. Zhou, Y. Wu, L.-m. Cao and J. Yang, Unraveling the Beneficial Electrochemistry of IrO_2/MoO_3 Hybrid as a Highly Stable and Efficient Oxygen Evolution Reaction Catalyst, *ACS Sustain. Chem. Eng.*, 2018, **6**, 4854-4862.
7. Y. Wu, R. Yao, Q. Zhao, J. Li and G. Liu, La-RuO_2 nanocrystals with efficient electrocatalytic activity for overall water splitting in acidic media: Synergistic effect of La doping and oxygen vacancy, *Chem. Eng. J.*, 2022, **439**, 135699.
8. L. Cao, Q. Luo, J. Chen, L. Wang, Y. Lin, H. Wang, X. Liu, X. Shen, W. Zhang, W. Liu, Z. Qi, Z. Jiang, J. Yang and T. Yao, Dynamic oxygen adsorption on single-atomic Ruthenium catalyst with high performance for acidic oxygen evolution reaction, *Nat. Commun.*, 2019, **10**, 4849.
9. L. Yang, G. Yu, X. Ai, W. Yan, H. Duan, W. Chen, X. Li, T. Wang, C. Zhang, X. Huang, J.-S. Chen and X. Zou, Efficient oxygen evolution electrocatalysis in acid by a perovskite with face-sharing IrO6 octahedral dimers, *Nat. Commun.*, 2018, **9**, 5236.

10. N. Zhang, C. Wang, J. Chen, C. Hu, J. Ma, X. Deng, B. Qiu, L. Cai, Y. Xiong and Y. Chai, Metal Substitution Steering Electron Correlations in Pyrochlore Ruthenates for Efficient Acidic Water Oxidation, *ACS Nano*, 2021, **15**, 8537-8548.

11. Z. Cheng, Y. Pi, Q. Shao and X. Huang, Boron-doped amorphous iridium oxide with ultrahigh mass activity for acidic oxygen evolution reaction, *Science China Materials*, 2021, **64**, 2958-2966.

12. J. Yang, Q. Shao, B. Huang, M. Sun and X. Huang, pH-Universal Water Splitting Catalyst: Ru-Ni Nanosheet Assemblies, *iScience*, 2019, **11**, 492-504.

13. P. Li, X. Duan, Y. Kuang and X. Sun, Iridium in Tungsten Trioxide Matrix as an Efficient Bi-Functional Electrocatalyst for Overall Water Splitting in Acidic Media, *Small*, 2021, **17**, 2102078.

14. O. Diaz-Morales, S. Raaijman, R. Kortlever, P. J. Kooyman, T. Wezendonk, J. Gascon, W. T. Fu and M. T. M. Koper, Iridium-based double perovskites for efficient water oxidation in acid media, *Nat. Commun.*, 2016, **7**, 12363.

15. J. Shan, C. Ye, S. Chen, T. Sun, Y. Jiao, L. Liu, C. Zhu, L. Song, Y. Han, M. Jaroniec, Y. Zhu, Y. Zheng and S.-Z. Qiao, Short-Range Ordered Iridium Single Atoms Integrated into Cobalt Oxide Spinel Structure for Highly Efficient Electrocatalytic Water Oxidation, *J. Am. Chem. Soc.*, 2021, **143**, 5201-5211.

16. Z. Wang, P. Wang, H. Zhang, W. Tian, Y. Xu, X. Li, L. Wang and H. Wang, Construction of hierarchical IrTe nanotubes with assembled nanosheets for overall water splitting electrocatalysis, *J. Mater. Chem. A*, 2021, **9**, 18576-18581.

17. J. Yin, J. Jin, M. Lu, B. Huang, H. Zhang, Y. Peng, P. Xi and C.-H. Yan, Iridium Single Atoms Coupling with Oxygen Vacancies Boosts Oxygen Evolution Reaction in Acid Media, *J. Am. Chem. Soc.*, 2020, **142**, 18378-18386.

18. L. C. Seitz, C. F. Dickens, K. Nishio, Y. Hikita, J. Montoya, A. Doyle, C. Kirk, A. Vojvodic, H. Y. Hwang, J. K. Norskov and T. F. Jaramillo, A highly active and stable $IrO_x/SrIrO_3$ catalyst for the oxygen evolution reaction, *Science*, 2016, **353**, 1011-1014.

19. Q. Qin, H. Jang, Y. Wang, L. Zhang, Z. Li, M. G. Kim, S. Liu, X. Liu and J. Cho, Gettering La Effect from La_3IrO_7 as a Highly Efficient Electrocatalyst for Oxygen Evolution Reaction in Acid Media, *Adv. Energy Mater.*, 2021, **11**, 2003561.